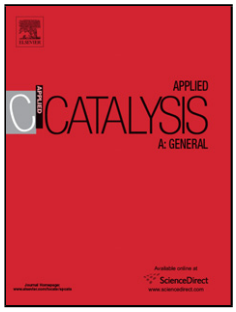

Title: Hydrogenation of Methyl Acetate to Ethanol over a Highly Stable Cu/SiO_2 Catalyst: Reaction Mechanism and Structural Evolution

Author: Xiumin Huang Meng Ma Shu Miao Yanping Zheng Mingshu Chen Wenjie Shen

PII: S0926-860X(16)30592-0
DOI: http://dx.doi.org/doi:10.1016/j.apcata.2016.12.006
Reference: APCATA 16091

To appear in: *Applied Catalysis A: General*

Received date: 22-6-2016
Revised date: 22-11-2016
Accepted date: 7-12-2016

Please cite this article as: Xiumin Huang, Meng Ma, Shu Miao, Yanping Zheng, Mingshu Chen, Wenjie Shen, Hydrogenation of Methyl Acetate to Ethanol over a Highly Stable Cu/SiO2 Catalyst: Reaction Mechanism and Structural Evolution, Applied Catalysis A, General http://dx.doi.org/10.1016/j.apcata.2016.12.006

Hydrogenation of Methyl Acetate to Ethanol over a Highly Stable Cu/SiO_2 Catalyst: Reaction Mechanism and Structural Evolution

Xiumin Huang[a,*], Meng Ma[a], Shu Miao[a], Yanping Zheng[b], Mingshu Chen[b], Wenjie Shen[a,*]

[a]*State Key Laboratory of Catalysis, Dalian Institute of Chemical Physics, Chinese Academy of Sciences, Dalian 116023, China.*

[b]*State Key Laboratory of Physical Chemistry of Solid Surfaces, Department of Chemistry, Xiamen University, Xiamen 361005, China.*

**Corresponding authors. Email addresses: hxiumin@dicp.ac.cn; shen98@dicp.ac.cn*

Graphical Abstract

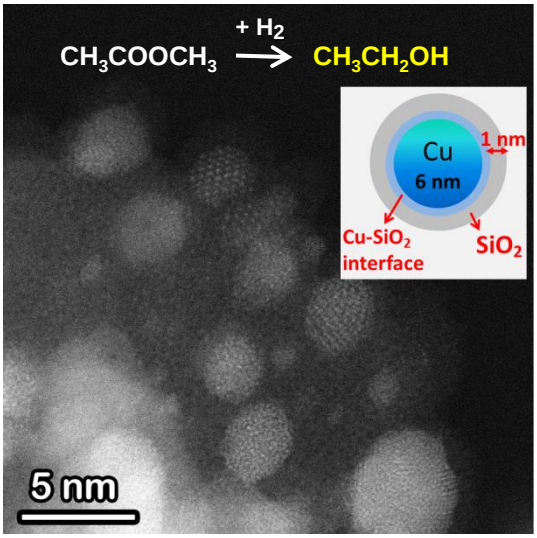

Research Highlights

- A core-shell structured Cu/SiO_2 catalyst with a copper particle of 4-7 nm and a SiO_2 shell of 1 nm was developed.
- The catalyst was highly active and stable for methyl acetate hydrogenation at 523 K. Methyl acetate conversion reached at 95% while the selectivity towards ethanol and methanol approached ~95%.
- The number of surface Cu^+ sites increased during the course of reaction due to the competitive adsorption of methyl acetate and hydrogen.
- A proper $Cu^+/(Cu^0+Cu^+)$ ratio is the prerequisite for achieving a higher catalytic performance of durable copper catalysts.

Abstracts

A Cu/SiO_2 catalyst with a core-shell structure was found to be highly active and stable for the hydrogenation of methyl acetate to ethanol during 96 hours reaction test at 523 K; MA conversion reached at 95% while the selectivity towards the major products (ethanol and methanol) approached ~95%. Structural analysis revealed that most copper particles in the hydrogen-reduced Cu/SiO_2 catalyst had sizes of 3-7 nm and were coated with a thin layer of silica, forming a core-shell structure. The average size of copper particles and the core-shell structure kept unchanged in the spent catalyst, but the $Cu^+/(Cu^0+Cu^+)$ ratio increased during the course of reaction, probably because of the electronic interaction between copper surface and methyl acetate under the reaction conditions. Accordingly, the outstanding stability of the Cu/SiO_2 was ascribed to the combination of geometric effect and electronic interaction. Mechanistic and kinetic studies have identified that ethyl acetate was formed through trans-esterification of initially produced ethanol with methyl acetate, while the subsequent hydrogenation of ethyl acetate to ethanol proceeded very fast. The $Cu^+/(Cu^0+Cu^+)$ ratio played a crucial role in reaction network; MA could adsorb equally on Cu^0 and Cu^+ sites while the activation of molecular hydrogen occurs only on the Cu^0 site. Therefore, a rather stable performance could be attained with the increase in the $Cu^+/(Cu^0+Cu^+)$ ratio during the course of reaction as long as the reaction is kinetically controlled by MA adsorption.

Keywords: Cu/SiO_2 catalyst; Core-shell structure; Methyl acetate; Hydrogenation; Stability.

1. Introduction

Ethanol is an important industrial feedstock for the synthesis of fine chemicals and is also used as fuels either directly or blended with gasoline. Recently, an integrated process for the production of ethanol from dimethyl ether (DME) was proposed, which is characterized by the use of cheap catalysts and the high reaction efficiency [1-3]. It consists of DME carbonylation to methyl acetate (MA) on zeolites and methyl acetate hydrogenation to ethanol over copper catalysts. DME carbonylation to MA occurred over mordenites with rather high selectivity and stability [4-9]; while MA hydrogenation to ethanol could be attained by using copper catalysts [1, 10, 11], primarily because they are highly active for C=O bond hydrogenation but much less active for C-C bond cleavage [12]. Mechanistic and kinetic

studies on MA hydrogenation have suggested that MA dissociated into methoxy and acetyl species upon adsorption on the copper catalysts; the CH_3O* species were readily converted into CH_3OH while the acetyl species adsorbed strongly on the catalyst surface, leaving hydrogenation of acetyls as the rate-determining step [10].

Cu/SiO_2 catalysts are typically used for MA hydrogenation at relatively higher copper loadings (> 30 wt.%) in order to promote the overall reaction efficiency. However, sintering of copper particles at elevated temperatures and under hydrogen atmosphere caused rapid deactivation of the Cu/SiO_2 catalysts. With this regard, enhancing copper-silica bonding becomes the crucial issue for maintaining their higher dispersion at high copper loadings and to alleviate their sintering under hydrogenation reaction conditions. For example, highly dispersed Cu particles with an average diameter of about 6 nm not only exhibited a much higher activity but also were rather resistance to sintering during glycerol hydrogenolysis [13, 14]. This was due to a strong interaction between Cu^{2+} and silica in the as-calcined sample through the formation of copper phyllosilicates. Surface modification of SiO_2 has been commonly adapted to enhance its chemical bonding with copper particles. Doping of SiO_2 surface with B_2O_3 [15-17], La_2O_3 [14, 18], NiO [19] and CeO_2 [20] all alleviated Cu sintering to some extents in Cu/SiO_2 catalysts for the hydrolysis of dimethyl oxalate or methyl acetate. However, the interaction mechanism between copper and silica and their structural variation under the hydrogenation reaction conditions are rarely examined.

In this work, we developed a core-shell structured Cu/SiO_2 catalyst with a copper loading of 38 wt.% and examined the structural evolution of the copper particles during MA hydrogenation. The Cu/SiO_2 catalyst showed excellent activity and stability towards methyl acetate hydrogenation to ethanol at 523 K, and the surface $Cu^+/(Cu^0+Cu^+)$ ratio played an essential role in the adsorption and activation of methyl acetate and hydrogen.

2. Experimental

2.1. Catalyst preparation

The Cu/SiO_2 catalyst was prepared by a precipitation-gel method, similar to a previous procedure [13]. 6.8 g $Cu(NO_3)_2 \cdot 6H_2O$ was dissolved into 57 ml deionized water; 25 mL 5 M NaOH aqueous solution was then added at a rate of 0.7 ml/min under vigorous stirring at room temperature with a final pH value of ~12.0, forming a blue precipitate. 4.18 g silica (Degussa A 200) was mixed with the slurry at

room temperature, and the mixture was further aged at 363 K for 4 h. The resulting solid was collected by filtration, thoroughly washed with hot water, dried at 393 K overnight, and finally calcined at 723 K for 3 h in air. The actual loading of copper was 38.3 wt. % measured by ICP analysis.

2.2. Catalytic tests

Hydrogenation of methyl acetate was tested with a fixed-bed stainless steel tubular reactor with an inner diameter of 8 mm. 300 mg catalysts (40-60 mesh) were loaded and reduced with pure H_2 (18 mL/min) at 573 K for 5 h. After the temperature was lowered to 423 K, the reactor system was pressurized to 1.0 MPa at a H_2 flow rate of 34 mL/min. Liquid methyl-acetate was injected through a micro-pump at a flow rate of 4 μl/min, corresponding to a MA concentration of ～3.0 vol.% in the feed stream. The reaction was then tested at desired temperatures (493-528 K). All the pipelines were heated at 353 K to avoid the condensation of the reactants and products. The exit stream from the reactor was analyzed by an online gas chromatograph (Agilent 6890N) equipped with a thermal conductivity detector (TCD) and a flame ionization detector (FID). An inert N_2 was adapted to maintain a constant flowrate in the reaction order tests. Conversion of MA is calculated via the amount of methyl acetate reacted divided by the amount of methyl acetate in the feed stream. The selectivity of a product is calculated as the stoichiometric number multiplies the mole amount of this product and then divided by the total number of products formed (the sum of the stoichiometric number multiplies the mole amount of each product). All the reaction data in this work was carefully checked by making carbon balance. The hydrogen-reduced and spent samples were collected after passivation in a 1% O_2/N_2 flow at room temperature for further characterizations.

2.3. Catalyst characterizations

The copper loading was measured by inductively coupled plasma atomic emission spectroscopy (ICP-AES) on a Plasma-Spec-II instrument. 20 mg as-calcined CuO/SiO_2 sample was dissolved in concentrated hydrochloric acid and hydrogen fluoride, and the mixture was diluted with water to meet the detection range of the instrument.

The specific surface area and pore size of the as-calcined CuO/SiO_2 sample was measured by nitrogen adsorption-desorption isotherms using an Autosorb-1 instrument (Quantachrome, USA) at 77 K. Before measurement, the sample was degassed in vacuum at 573 K for 6 h. The specific surface area (S_{BET}) was estimated by the Brunauer-Emmett-Teller (BET) method, while the mesopore size distribution was

calculated from the desorption branch of the isotherm using the BJH method.

Power X-ray diffraction (XRD) patterns were recorded on a D/Max-2500/PC diffractometer (Rigaku, Japan) using a Cu Kα (λ = 0.154 nm) radiation source that operated at 40 kV and 200 mA. In situ XRD measurements were tested with the same instrument at 40 kV and 300 mA. 200 mg CuO/SiO_2 sample was pressed into a flake, mounted in a chamber, exposed to a 5% H_2/N_2 mixture (30 mL/min) and gradually heated to 573 K for 5 h at a rate of 5 K/min. XRD patterns were recorded at desired temperatures. The average crystallite sizes of CuO and Cu^0 in the as-calcined and hydrogen-reduced samples was estimated from the full widths at half maxima of their typical diffractions according to the Scherrer's equation.

Transmission electron microscopy (TEM) images were recorded on a FEI Tecnai G2 Spirit microscope operated at 120 kV; High-resolution TEM (HRTEM) images were recorded on a JEM-2100 microscope; HAADF-STEM images were recorded on a JEM-ARM200F microscope. The specimen was prepared by ultrasonically dispersing the solid sample into ethanol, and droplets of the suspensions were deposited on a carbon-coated copper or molybdenum grid and then dried in air.

Temperature-programmed reduction with hydrogen (H_2-TPR) and dissociative N_2O titration was performed with an AutoChem II 2920 instrument (Micromeritics) equipped with a TCD. 30 mg CuO/SiO_2 sample was pretreated at 723 K (10 K/min) for 2 h with a 20% O_2/N_2 mixture (30 mL/min) to remove the surface impurities. After cooling down to room temperature and purging with Ar, the sample was reduced with a 5% H_2/N_2 mixture (30 mL/min) at 573 K at a rate of 5 K/min for 1 h. The resulting Cu/SiO_2 catalyst was purged with Ar flow and exposed to a 10% N_2O/He mixture (30 mL/min) at 363 K for 30 min. A second TPR run was then conducted by heating the sample to 573 K at a rate of 5 K/min and under the flow of a 5% H_2/N_2 mixture (30 mL/min). The dispersion (D) and average size (d) of copper particles were estimated according to the following equations:

$$D = (2 \cdot A_2/A_1) \times 100\%, \quad d = 0.5\ A_1/A_2 = 1/D\ (nm)$$

Where A_1 and A_2 represented the amounts of hydrogen consumed during the first and second TPR runs, respectively. The average diameter (d) of copper particles was calculated from A_1 and A_2 by assuming 1.46×10^{19} copper atoms per m^2 and a molar stoichiometry of $N_2O/Cu^s = 0.5$, in which Cu^s means the copper atoms on the surface [21, 22].

Temperature-programmed desorption of methyl acetate (MA-TPD) on the Cu/SiO_2 catalysts was also conducted on the AutoChem II 2920 instrument. The generation of Cu(0) sample was achieved by

reducing the as-calcined CuO/SiO_2 sample (30 mg) with a 5% H_2/N_2 mixture at 573 K for 1 h; while the Cu(+) sample was produced by further exposing the above Cu(0) sample to a mixture of 10% N_2O/He at 363 K for 0.5 h. The obtained Cu(0) and Cu(+) samples were cooled down to 313 K, purged with Ar (30 mL/min) for 0.5 h; and then exposed to a 2% MA/He mixture (20 mL/min) for 40 min. After sweeping with He (30 mL/min) for 30 min to remove the physically adsorbed species, the samples were heated to 823 K at a rate of 5 K/min and the desorbed species were monitored with a TCD.

Temperature-programmed oxidation (TPO) of the spent catalysts was conducted with a U-type quartz tubular reactor connected to an online mass spectrometer (OmniStar 200, Balzers). 22 mg spent sample was heated to 873 K at a rate of 10 K/min under He flow (30 mL/min) and kept at that temperature for 1 h. After cooling down to room temperature, the sample was exposed to a 20% O_2/He mixture (30 mL/min) and heated to 873 K at a rate of 10 K/min. The evolution of CO_2 (m/e=44), H_2O (m/e=18), and CO (m/e=28) was monitored by the mass spectrometer.

X-ray photoelectron spectroscopy (XPS) and Auger electron spectroscopy measurements were carried out in a UHV system using an Al Kα radiation source (hv=1486.6 eV) and an Omicron Sphera II hemispherical electron energy analyzer. Both the as-calcined and spent samples were pressed into a thin disk and reduced with pure H_2 at 483 and/or 573 K for 2 h; the sample was then transferred into the XPS analysis chamber without exposing to air. The binding energies were calibrated using the Si_{2p} peak at 103.6 eV as the reference. Deconvolution of Cu LMM Auger spectra was conducted by keeping the Lorentzian/Gaussian ratio of the baseline constant at 1:99 and the binding energy of Cu^+ being 4 eV higher than that of Cu^0.

3. Results and discussion

3.1 Physical and Chemical properties of the Cu/SiO_2 catalysts

Fig. 1 show the N_2 adsorption-desorption isotherm of the SiO_2 support, the as-calcined CuO/SiO_2 sample and the pore size distribution. The surface area was about 186 m^2/g and 196 m^2/g for bare SiO_2 and CuO/SiO_2 sample respectively. Besides the original mesopore of 26.1 nm caused by the accumulation of SiO_2 particles, no apparent additional mesopores appeared. However, the dV(logD) value of the CuO/SiO_2 sample was not equal to zero and was much higher than that of the SiO_2 support at the starting point (inset Fig. 1b), suggesting that pores below 3 nm were generated on the CuO/SiO_2

catalyst. Fig. 2 shows the XRD patterns of the Cu/SiO_2 catalysts. The CuO/SiO_2 sample showed characteristic diffraction lines of CuO with a mean crystalline size of ~ 5.5 nm. After hydrogen reduction at 573 K for 5 h, only the metallic Cu crystallite was detected. Fig. 3 displays the TEM images of the as-calcined CuO/SiO_2 sample. Both rounded particles of about 20 nm and nanorods with lengths up to several hundreds of nanometers (200-500 nm) were clearly observed. HRTEM analysis on the nanorods further identified that the CuO particles were arranged in a pearl-threaded pattern and surrounded by a thin layer of amorphous SiO_2. The amorphous layer was clearly seen as the incident angle of electrons was rotated for 30^o, suggesting the formation of a core-shell structure on the rod-like section. The formation of such a rod-like structure might be assigned to the arrangement of CuO particles, which originated from the $Cu(OH)_2$ precipitate that are prone to form one-dimensional structure under highly basic solutions during the preparation. Fig. 4 shows the TEM images of the Cu/SiO_2 catalyst that was obtained by hydrogen reduction at 573 K of the as-calcined CuO/SiO_2 sample. Apparently, the Cu/SiO_2 catalyst inherited the morphology of the precursor. Highly dispersed Cu particles with a diameter of ~5 nm were clearly observed; most copper particle had sizes in the range of 4-7 nm; small particles of 1-3 nm and large particles of ~10 nm were also observed occasionally. More importantly, most copper particles were uniformly coated with a thin layer of silica with a thickness of ~1 nm, confirming the core-shell structure on the highly dispersed copper particles. The exact formation mechanism of the core-shell structure was not clear, but it could be assumed that $Cu(OH)_2$ precipitate was initially formed in the strong basic solution, and the later added SiO_2 particles were partly dissolved and negatively charged under such a high pH solution [18, 23]. The strong electronic interaction between the positively charged $Cu(OH)_2$ particles and the negatively charged SiO_2 species resulted in the enwrap of the $Cu(OH)_2$ precipitate during the aging process and therefore the core-shell structure in the CuO/SiO_2 and Cu/SiO_2 samples. To get a clear point of view whether there are pathways to the core particles through the SiO_2 layer, the CuO/SiO_2 powder sample was immersed in aqueous H_2SO_4 solution with a PH value of ~ 1 at room temperature, the CuO particles can be almost dissolved after 2 h, suggesting that the CuO particles are not totally covered by SiO_2. Some cracks or micropores should be presented in the thin silica layers and were responsible for the reactant molecules to access the Cu nanoparticles, in consistent with the adsorption-desorption results that pores below 3 nm were exhibited on the CuO/SiO_2 catalyst.

Fig. 5 shows the H_2-TPR profile of the as-calcined CuO/SiO_2 sample. The intense reduction peak at

521 K was ascribed to the reduction of CuO. However, the amount of H_2 consumed (4.67 mmol/g) was lower than the stoichiometric value (5.46 mmol/g) required for the complete reduction of CuO to metallic copper. This indicates there presents hard-reducible Cu^{2+} species, which are most likely those that strongly interacted with the silica support at the CuO-SiO_2 interface. Therefore, the broad reduction is actually a collective contribution from the transformation of CuO to Cu^0 and Cu^{2+} species at the CuO-SiO_2 interface to Cu^+. Estimated from the amount of H_2 consumed, 71.1% copper species could be fully reduced into Cu^0 while 28.9% copper species were only partially reduced into Cu^+. N_2O titration on the hydrogen-reduced Cu/SiO_2 sample indicated that the dispersion of Cu was 16.0%, equaling to a mean particle size of 6.2 nm.

Fig. 6 shows the XPS spectra recorded during hydrogen reduction of the as-calcined CuO/SiO_2 sample. The binding energy of Cu $2p_{3/2}$ at 934.7 eV, together with the characteristic shakeup 2p → 3d satellite peaks at 942-944 eV [21], evidenced the presence of Cu^{2+}. Upon hydrogen reduction at 573 K, the satellite peaks vanished while new binding energies at 952.9 and 932.9 eV appeared, evidencing that the Cu^{2+} species were converted into Cu^+ and/or Cu^0 species [15, 18, 24, 25]. Because of the identical binding energies between Cu^+ and Cu^0, Cu LMM X-ray excited Auger spectroscopy was adapted to distinguish these copper species. The binding energy at 572.2 eV was assigned to Cu^+ while that at 568.2 eV was ascribed to Cu^0 [18, 25]. Accordingly, the remaining Cu^+ species, with a $Cu^+/(Cu^0+Cu^+)$ ratio of 28.1%, could be attributed to those strongly interacted or incorporated into silica at the Cu-SiO_2 interface, which is in good agreement with the H_2-TPR result that 28.9% Cu^+ species presented on the hydrogen-reduced Cu/SiO_2 sample. The absence of Cu^+ species by XRD technique for the hydrogen-reduced sample might be due to that the Cu species strongly interacted with SiO_2 layer was amorphous, or it was located on the catalyst surface or the Cu^+ particle was too small to be detected, because XRD technique detects only the crystalline phase in the bulk while XPS probes the surface species both in crystalline and amorphous form. The surface Cu/Si atomic ratio was estimated to be 0.12 on the as-calcined CuO/SiO_2 catalyst by XPS, far below the theoretical Cu/Si ratio of 0.58 based on ICP analysis. Considering the relatively small copper size of 5-6 nm, the prominent difference in Cu/Si ratio as measured by XPS and ICP methods inferred that silica was dominated on the catalyst surface, an auxiliary evidence for the formation of a core-shell structure.

3.2. Hydrogenation of methyl acetate over the Cu/SiO_2 *catalyst*

Table 1 summarizes the reaction results of methyl acetate hydrogenation over the Cu/SiO_2 catalyst at 493-528 K. The main products were ethanol, methanol and ethyl acetate (EtOAc), among which ethyl acetate was formed through trans-esterification of the initially formed ethanol with methyl acetate; the by-products included acetaldehyde and alkanes in traceable amounts. The conversion of MA increased dramatically from 26.5% at 493 K to 96.2% at 528 K; the corresponding selectivity of EtOH increased prominently from 30.8% to 61.7% while the selectivity of EtOAc dramatically decreased from 32.7% to 2.5%, suggesting that hydrogenation of EtOAc occurred as the major reaction. As a consequence, the total selectivity of EtOH and EtOAc kept nearly constant at ~ 64% while the selectivity of MeOH only marginally decreased from 36.4% to 33.6% with raising the temperature. Concerning the by-products, CH_4 was the only detectable byproduct at 493 K with a selectivity of 0.2%, while ethane and acetaldehyde were formed at 518 K and their total selectivity slightly increased to 2.2% at 528 K.

Reaction kinetic of MA hydrogenation on the Cu/SiO_2 catalyst was then examined. The effect of internal diffusion is usually negligible at the used submillimeter particles of 0.25-0.35 mm (40-60 mesh), while the external mass-transfer resistance on the reaction was precluded through primary tests (Table 2). Fig. 7 shows the variation in product distribution at different MA conversions at 498 K. The conversion of MA showed an almost linear correlation with the contact time (W/F) passing through the origin, indicating that MA hydrogenation is a typical heterogeneous catalytic surface reaction over the Cu/SiO_2 catalyst. At MA conversions less than 28%, the selectivity of EtOH continuously decreased while the selectivity of ethyl acetate increased with increasing the MA conversion. This suggests that EtOH is the primary product (Equation 1) while ethyl acetate is the secondary product, which was produced through trans-esterification of methyl acetate with the initially produced EtOH (Equation 2). As the conversion of MA was above 28%, the selectivity of EtOH increased while that of EtOAc decreased with increasing MA conversion. This means that hydrogenation of ethyl acetate occurred predominantly and ethanol was produced as the secondary product (Equation 3) at this stage. Control experiments for hydrogenation of methyl acetate and ethyl acetate further confirmed that hydrogenation of ethyl acetate proceeded much faster than that of methyl acetate over the Cu/SiO_2 catalyst (Table 3), as previously observed [11]. Under identical reaction conditions, the conversion of MA was only 26.5% with an ethanol selectivity of 30.8% at 493 K, whereas the conversion of EA approached 77.3% with an EtOH selectivity of 99.4%. At 513 K, MA conversion increased to 81.1% with a moderate increase in ethanol selectivity (52.9%), while EA conversion attained 91.8% with an

ethanol selectivity of 98-99%. Therefore, it is reasonable to conclude that the faster hydrogenation of ethyl acetate to ethanol was responsible for the greatly enhanced EtOH selectivity at higher MA conversions. It is worth noting that the selectivity of CH_3OH was essentially independent of MA conversion. CH_3OH can be produced through hydrogenation of MA and trans-esterification of MA with EtOH, but its amount is only correlated with the amount of MA converted, keeping a constant selectivity in the product slate.

Concerning the minor byproducts, the selectivity of acetaldehyde decreased at lower MA conversions, indicating that it was a primary product through hydrogenation of the CH_3CO^* fragment adsorbed on the catalyst surface (equation 1-1), as previously proposed [10], and the subsequent hydrogenation of acetaldehyde to EtOH (equation 1-2) proceeded very fast [26]. At higher MA conversions, however, the selectivity of acetaldehyde increased, suggesting that acetaldehyde was also formed as a secondary product through EtOH dehydrogenation (Equation 1-2). Although in traceable amounts, alkanes were formed at 493 K and their selectivity showed an inverse volcano pattern with MA conversion. Since CH_4 was the only detected alkane at lower MA conversions and its selectivity decreased with decreasing MA conversion, it could be inferred that CH_4 acted as the primary product probably formed by direct hydrogenation of the CH_3^* fragments in MA (equation 4). Meanwhile, the formation of traceable AcOH further evidenced the occurrence of this reaction route. The selectivity of C_2H_6 among alkanes increased with MA conversion in the whole range, suggesting that ethane was a secondary product. To identify the formation route of C_2H_6, hydrolysis of ethanol was tested on the Cu/SiO_2 catalyst (Table 3). Ethane was formed at 498 K although the conversion of ethanol was only 0.6%, and its amount increased as the reaction temperature further ramped to 518 K. This clearly evidences that ethane was produced by ethanol hydrolysis (equation 5). The fact that there was no detectable CH_4 in the outlet stream during ethanol hydrolysis excluded the occurrence of ethanol decomposition under the current reaction conditions. However, acetaldehyde was formed as a major product with a selectivity of ~65%, suggesting that EtOH dehydrogenation occurred under the current reaction conditions. Besides, blank tests for MA hydrogenation, MA decomposition and hydrolysis of ethanol revealed the absence of any products below 523 K, indicating that all the involved reactions were took place on the catalyst surface. On the basis of these kinetic results, the surface reaction network for MA hydrogenation was illustrated in Scheme 1.

$CH_3COOCH_3 + 2H_2 \rightarrow CH_3CH_2OH + CH_3OH$ (1)

$CH_3COOCH_3 + H_2 \rightarrow CH_3CHO + CH_3OH$ (1-1)

$CH_3CHO + H_2 \rightleftharpoons CH_3CH_2OH$ (1-2)

$CH_3COOCH_3 + CH_3CH_2OH \rightarrow CH_3COOCH_2CH_3 + CH_3OH$ (2)

$CH_3COOCH_2CH_3 + 2H_2 \rightarrow 2CH_3CH_2OH$ (3)

$CH_3COOCH_3 + H_2 \rightarrow CH_4 + CH_3COOH$ (4)

$CH_3CH_2OH + H_2 \rightarrow CH_3\text{-}CH_3 + H_2O$ (5)

Fig. 8a shows the effect of H_2 partial pressure on the reaction rates and the product selectivity at 513 K. As increasing hydrogen pressure from 0.4 to 1.0 MPa, the reaction rate of MA increased linearly from 3.6 to 8.8 mmol/(g_{cat}·h); the selectivity of ethanol increased remarkably while the selectivity of ethyl acetate deceased dramatically. This indicates that hydrogenation of ethyl acetate to ethanol occurred more significantly as raising H_2 partial pressure. The reaction order of 0.9 with respect to hydrogen suggests that hydrogen molecule was associatively adsorbed on copper surface, supposing the reaction follows a Langmuir-Hinshelwood model [10]. Fig. 8b shows the effect of MA partial pressure on the reaction rate of MA and the product selectivity at 523 K. The reaction rate showed a typical volcano shape with respect to MA partial pressure. As MA partial pressure was less than 50 kPa (i.e. $MA/H_2 < 0.05$), the conversion rate of MA increased continuously with increasing MA partial pressure, indicating the adsorption of MA might be the rate-determining step. As such, increasing MA concentration in the reaction stream would cause more MA species adsorbed on the Cu surface, showing a reaction order of 0.65. This is in accordance with a previous observation that methyl acetate was adsorbed dissociatively at lower partial pressures with an apparent reaction order of about 0.5 [10]. At MA partial pressures higher than 50 kPa ($MA/H_2 > 0.05$), however, the reaction rate of MA declined significantly with increasing MA concentration in the feed stream. Later work on MA-TPD evidenced that MA adsorption took place on both Cu^0 and Cu^+ sites of the hydrogen-reduced Cu/SiO_2 catalyst. The adsorption of H_2 on Cu^0 surface is generally accepted and has been verified by H_2-TPA and H_2-TPD methods. It was demonstrated that H_2 adsorption was a strongly activated process started at 200 K on Cu/Al_2O_3 catalyst [27], while H_2 desorption corresponding to chemisorbed H_2 on the metallic Cu surface of Cu/SiO_2 and Cu/Al_2O_3 happened below 373 K [18, 27]. Therefore, it can be inferred that in an atmosphere with both MA and H_2 presented, competitive adsorption of MA and H_2 happened on

the Cu^0 sites of the Cu/SiO_2 catalyst. Accordingly, too much MA adsorption on the active Cu^0 site decreased the adsorption or activation of hydrogen, thus lowering the overall reaction rate. The reaction order of -0.89 with respect to MA suggested that MA was dominantly adsorbed on the catalyst surface in a molecular form under the reaction conditions, differing from the dissociative adsorption at lower MA partial pressure. The competitive adsorption of hydrogen and methyl acetate implies that hydrogen molecule was activated on copper surface in the reaction network, instead of gaseous molecular hydrogen.

3.3. Structural evolution of the Cu/SiO_2 catalyst during MA hydrogenation

Fig. 9 shows the result of stability test of the Cu/SiO_2 catalyst for MA hydrogenation at 523 K for ~100 hours. The conversion of MA maintained at 95%; the selectivity for the major products (EtOH, MeOH and EA) approached ~98% while the selectivity for the minor products (acetaldehyde and alkanes) was about 2%. This demonstrates the rather high activity and stability of the current Cu/SiO_2 catalyst for MA hydrogenation. Fig. 10 shows the temperature-programmed desorption profile of the spent Cu/SiO_2 catalyst. The intense desorption of CO_2 and H_2O below 700 K under a He flow suggested that carbonaceous species were adsorbed on the catalyst surface. The subsequent temperature-programmed oxidation with a $20\%O_2/N_2$ flow did not produce appreciable CO_2 and no obvious consumption of O_2 was detected; this confirms that the carbon-containing deposits were completely removed during the treatment with an inert gas. That is, no hard coke was presented over the spent sample.

Fig. 2d shows the XRD pattern of the spent Cu/SiO_2 catalyst after passivation. The average crystalline size of metallic copper (4.7 nm) was quite close to that in the hydrogen-reduced sample just before reaction (5.0 nm). This suggests that there was no detectable sintering of copper particles during methyl acetate hydrogenation. However, a prominent diffraction line at 2-theta value of 36.4 appeared, corresponding to Cu_2O, indicating that part of the metallic copper was transformed into Cu_2O during the course of reaction. TEM/STEM analyses on the spent catalyst suggested that there was no apparent aggregation of Cu particles during MA hydrogenation (Fig. 11), in consistent with the XRD result. Most copper particles were still in the size range of 4-7 nm, together with few small particles of 1-3 nm and large ones of ~10 nm. Moreover, the core-shell structure of a thin layer of SiO_2 on Cu particles was also observed. The H_2-TPR profile of the spent Cu/SiO_2 catalyst was shown in Fig. 5. The passivated sample after the stability test was treated with a 20% O_2/N_2 mixture at 723 K for 2 h, followed by

H_2-TPR and N_2O titration measurements. The dispersion of Cu was 15.8%, equaling to a mean particle size of 6.3 nm. This is comparable with the hydrogen-reduced sample prior to the reaction with a Cu dispersion of 16.0%. All these results confirmed that copper particles kept rather stable under MA hydrogenation conditions without obvious change in size.

The XPS spectra of the spent Cu/SiO_2 catalyst were compared in Fig. 6. For the passivated spent sample, the main binding energies of Cu_{2p} at 932.9 and 952.9 eV represented Cu^+/Cu^0 species, while the minor satellite peak for Cu^{2+} indicated surface oxidation during the passivation treatment. Hydrogen treatment at 483 K totally removed those surface oxidized species and fully regenerated the catalyst surface, leaving Cu^+ and Cu^0 as the surface copper species. However, the $Cu^+/(Cu^0+Cu^+)$ ratio on the regenerated catalyst (38.9%) is much higher than that on the hydrogen-reduced Cu/SiO_2 catalyst prior to reaction (28.1%). As the passivated spent sample was further reduced at 573 K with hydrogen, the $Cu^+/(Cu^0+Cu^+)$ ratio decreased to 31.6%; which is still higher than that on the hydrogen-reduced Cu/SiO_2 catalyst. This implies that a substantial amount of Cu^+ species were generated during the course of reaction, probably involving the surface oxidation of copper particles and/or copper species at the $Cu\text{-}SiO_2$ interface by methyl acetate.

It is generally accepted that the Cu^+ site stabilizes methoxy group while the Cu^0 site catalyzes hydrogenation of acyl species during MA hydrogenation [15, 24, 25, 28-30]. To elucidate the catalytic roles of Cu^0 and Cu^+ species in MA hydrogenation, temperature-programmed desorption of MA on the Cu/SiO_2 catalysts containing different copper species was examined (Fig. 12). It should be noted that the Cu(0) sample contained about 28.9% Cu^+ owing to the presence of copper strongly interacted with the silica support, while the Cu(+) sample composed of nearly 100% Cu^+ on the surface. The two samples showed almost identical MA desorption patterns at 528 K, suggesting that MA adsorbed equally on the Cu^0 and Cu^+ sites of the copper particles. Here, the similar adsorption behavior of MA over Cu^0 and Cu^+ sites implies that their ability for H_2 activation would control the overall activity.

As demonstrated by the kinetic measurements, MA and H_2 were competitively adsorbed on the copper sites at the beginning of the reaction. It has been generally known that hydrogen molecules adsorbed only on metallic copper with a weak interaction. Desorption of H_2 took place in a temperature range of 270-350 K [18, 27]. Our experiment data showed MA adsorbed equally on Cu^+ and Cu^0 sites and MA desorption occurred at a temperature of 528 K. This indicates that the adsorption of MA on Cu^0 site was much stronger than that of H_2. As a consequence, Cu^0 site covered by MA was gradually oxidized

into Cu^+ during the hydrogenation process through electronic chemical interaction between metallic copper surface and the strongly adsorbed oxygen-containing groups of the esters.

In catalytic reactions, the promotion or degradation in activity is eventually controlled by the rate determining step at the used reaction conditions. During the course of stability test shown in Fig. 9, the surface $Cu^+/(Cu^0+Cu^+)$ ratio increased from 28.1% to 38.9%, but rather high stability of the reaction was maintained. This can be explained by the lower MA/H_2 molar ratio adopted here. At MA/H_2 molar ratio of 0.30, MA adsorption acted as the rate-determining step based on the kinetic study shown in Fig. 8b. Considering the fact that MA adsorbed equally on the Cu^+ and Cu^0 sites, the catalytic activity would be kept unchanged provided that newly generated Cu^+ sites were still responsible for MA activation and the remaining Cu^0 sites were still sufficient for hydrogen activation, as shown in Fig. 9. If the reaction is kinetically controlled by H_2 activation, for example, at higher MA/H_2 ratios in the feed stream, a gradual enhancement in the number of Cu^+ sites on the catalyst surface would hinder the activation of H_2 on metallic copper surface and consequently caused deactivation. Therefore, a proper $Cu^+/(Cu^0+Cu^+)$ ratio is the prerequisite for achieving a higher catalytic performance, which is related with the adopted reaction conditions, in particular the MA/H_2 molar ratio. Moreover, the core-shell structure of the Cu/SiO_2 catalyst efficiently prohibited the aggregation of copper particles. The Cu^+ species formed during the course of reaction might also take some role on relieving the coagulation of copper particles owing to the fact that Cu^+ is more difficult to coagulation than that of Cu^0 [31]. That is, the outstanding stability of the Cu/SiO_2 catalyst is actually a combination of geometric and electronic effects.

4. Conclusions

A highly stable Cu/SiO_2 catalyst with a core-shell structure was prepared using a simple precipitation-gel method. TEM/STEM analyses on the as-calcined CuO/SiO_2 sample identified that most CuO particles were in the size range of 3-7 nm and coated with a thin layer of silica. 71% copper species in the core was loosely interacted with silica while 29% copper species at the $CuO\text{-}SiO_2$ interface was strongly interacted with silica. Upon hydrogen reduction at 573 K, the core CuO particles were fully reduced into metallic copper species while the Cu^{2+} species at the $CuO\text{-}SiO_2$ interface were only partially reduced into Cu^+, giving a $Cu^+/(Cu^0+Cu^+)$ ratio of 28.1%. The Cu/SiO_2 catalyst showed outstanding activity and stability for methyl acetate hydrogenation at 523 K for ~100 h on-stream; the

conversion of MA maintained at 95% with a total selectivity of 95% for ethanol and methanol. The size of copper particles kept unchanged and the core-shell structure of copper particles was preserved. However, the ratio of surface $Cu^{+}/(Cu^{0}+Cu^{+})$ increased to 38.9% due to the electronic interaction of copper particles and/or copper species at the Cu-SiO_2 interface with methyl acetate under the reaction conditions. Accordingly, the outstanding stability of the Cu/SiO_2 catalyst was assigned to a combination of geometric (the core-shell structure) and electronic (a proper $Cu^{+}/(Cu^{0}+Cu^{+})$ ratio) effects. This result offers a general strategy for the rational design of durable copper catalyst.

Acknowledgements

This work was supported by the National Key Basic Research Program of China (2013CB933100) and the National Natural Science Foundation of China (21533009).

References

[1] X.G. San, Y. Zhang, W.J. Shen, N. Tsubaki, ***Energy & Fuels*** 23 (2009) 2843-2844.

[2] X.G. Li, X.G. San, Y. Zhang, T. Ichii, M. Meng, Y.S. Tan, N. Tsubaki, ***ChemSusChem*** 3 (2010) 1192-1199.

[3] P. Haro, P. Ollero, A.L. Villanueva Perales, C. Reyes Valle, ***Energy*** 44 (2012) 891-901.

[4] P. Cheung, A. Bhan, G. J. Sunley, E. Iglesia, ***Angew. Chem. Int. Ed.*** 45 (2006) 1617-1620.

[5] P. Cheung, A. Bhan, G. J. Sunley, D. J. Law, E. Iglesia, ***J. Catal.*** 245 (2007) 110-123.

[6] J.L. Liu, H.F. Xue, X.M. Huang, P.H. Wu, S.J. Huang, S.B. Liu, W.J. Shen, ***Chin. J. Catal.*** 31 (2010) 729-738.

[7] H. Zhou, W.L. Zhu, L. Shi, H.C. Liu, S.P. Liu, S.T. Xu, Y.M. Ni, Y. Liu, L.N. Li and Z.M. Liu, ***Catal. Sci. Technol.*** 5 (2015) 1961-1968.

[8] Y.H. Liu, N. Zhao, H. Xian, Q.P. Cheng, Y.S. Tan, N. Tsubaki, X.G. Li, ***ACS Appl. Mater. Interfaces*** 7 (2015) 8398-8403.

[9] H.F. Xue, X.M. Huang, E. Ditzel, E.S. Zhan, M. Ma, W.J. Shen, ***Ind. Eng. Chem. Res.*** 52 (2013) 11510-11515.

[10] A.K. Agarwal, N.W. Cant, M.S. Wainwright, D.L. Trimm, ***J. Mol. Catal.*** 43 (1987) 79-92.

[11] M. A. Nata Santiago, M. A. S´anchez-Castillo, R. D. Cortright, J. A. Dumesic, ***J. Catal.*** 193(2000) 16-28.

[12] Z.W. Huang, F. Cui, J.J. Xue, J.L. Zuo, J. Chen, C.G. Xia, ***Catal. Today*** 183 (2012) 42-51.

[13] Z.W. Huang, F. Cui, H.X. Kang, J. Chen, X.Z. Zhang, C.G. Xia, ***Chem. Mater.*** 20 (2008) 5090-5099.

[14] Z.W. Huang, H.L. Liu, F. Cui, J.L. Zuo, J. Chen, C.G. Xia, ***Catal. Today*** 234 (2014) 223-232.

[15] Z. He, H.Q. Lin, P. He, Y.Z. Yuan, ***J. Catal.*** 277 (2011) 54-63.

[16] S. Zhao, H.R. Yue, Y.J. Zhao, B. Wang, Y.C. Geng, J. Lv, S.P. Wang, J.L. Gong, X.B. Ma, ***J. Catal.*** 297 (2013) 142-150.

[17] S.H. Zhu, X.Q. Gao, Y.L. Zhu, Y.F. Zhu, H.Y. Zheng, Y.W. Li, ***J. Catal.*** 303 (2013) 70-79.

[18] X.L. Zheng, H.Q. Lin, J.W. Zheng, X.P. Duan, Y.Z. Yuan, ***ACS Catal.*** 3 (2013) 2738-2749.

[19] A.Y. Yin, C. Wen, X.Y. Guo, W.L. Dai, K.N. Fan, ***J. Catal.*** 280 (2011) 77-88.

[20] C.L. Ye, C.L. Guo, J.L. Zhang, ***Fuel Process. Technol.*** 143 (2016) 219-224.

[21] C. J. G. Van Der Grift, A. F. H. Wielers, B. P. J. Joghi, J. Van Beijnum, M. De Boer, M. Versluijs-Helder, J. W. Geus, ***J. Catal.*** 131 (1991) 178-189.

[22] J. W. Evans, M. S. Wainwright, A. J. Bridgewater, D. J. Yong, ***Appl. Catal***. 7 (1983) 75-83.

[23] Z.W. Huang, F. Cui, J.J. Xue, J.L. Zuo, J. Chen, C.G. Xia, ***J. Phys. Chem. C*** 114 (2010) 16104-16113.

[24] L.F. Chen, P.J. Guo, M.H. Qiao, S.R. Yan, H.X. Li, W. Shen, H.L. Xu, K.N. Fan, ***J. Catal.*** 257 (2008) 172-180.

[25] J.L. Gong, H.R. Yue, Y.J. Zhao, S. Zhao, L. Zhao, J. Lv, S.P. Wang, X.B. Ma, ***J. Am. Chem. Soc***. 134 (2012) 13922-13925.

[26] P. Claus, M. Lucas, B. Lucke, ***Appl. Catal. A: Gen.*** 79 (1991) 1-18.

[27] H. Wilmer, T. Genger, O. Hinrichsen, ***J. Catal.*** 215 (2003) 188-198.

[28] J.W. Evans, M.S. Wainwright, N.W. Cant, D.L. Trimm, ***J. Catal.*** 88 (1984) 203-213.

[29] S.H. Zhu, X.Q. Gao, Y.L. Zhu, W.B. Fan, J.G. Wang, Y.W. Li, ***Catal. Sci. Technol.*** 5 (2015) 1169-1180.

[30] E.K. Poels, D.S. Brands, ***Appl. Catal. A: Gen.*** 191 (2000) 83-96.

[31] A.J. Marchi, J.L.G. Fierro, J. Santamaría, A. Mozón, ***Appl. Catal. A: Gen.*** 142 (1996) 375-386.

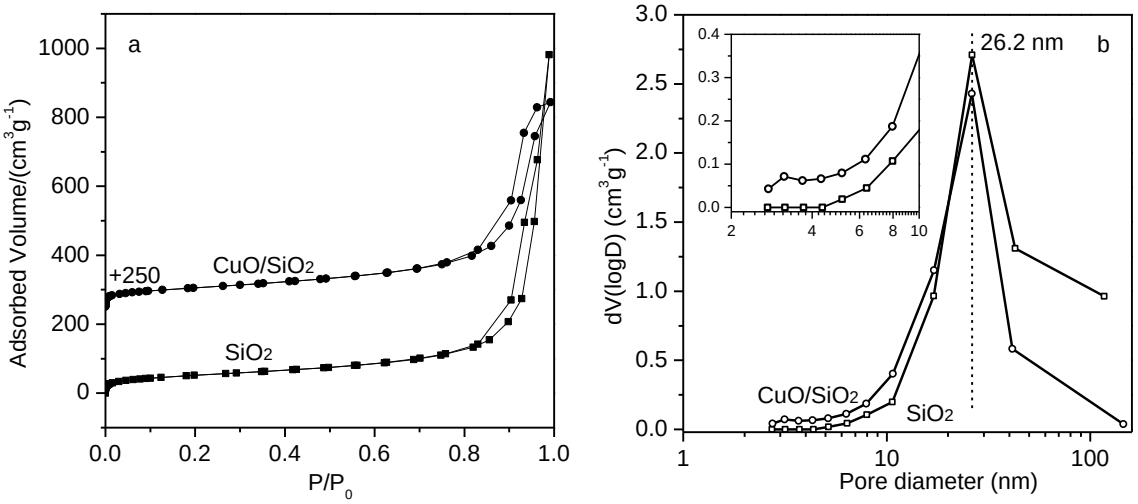

Figure 1. N_2 adsorption-desorption isotherm and pore size distribution of the bare SiO_2 and calcined CuO/SiO_2 sample. (a) N_2 adsorption-desorption isotherm (b) mesopore size distribution by BJH method.

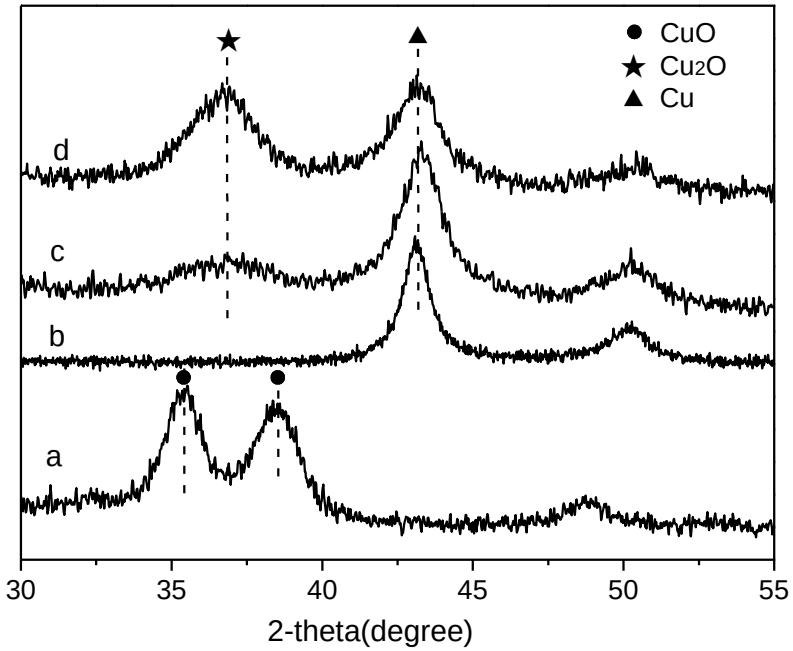

Figure 2. XRD patterns of (a) the as-calcined CuO/SiO_2 sample, (b) the hydrogen-reduced Cu/SiO_2 catalyst at 573 K, (c) the Cu/SiO_2 sample obtained by passivation of (b), and (d) the spent Cu/SiO_2 catalyst sample obtained by passivation after stability test for MA hydrogenation.

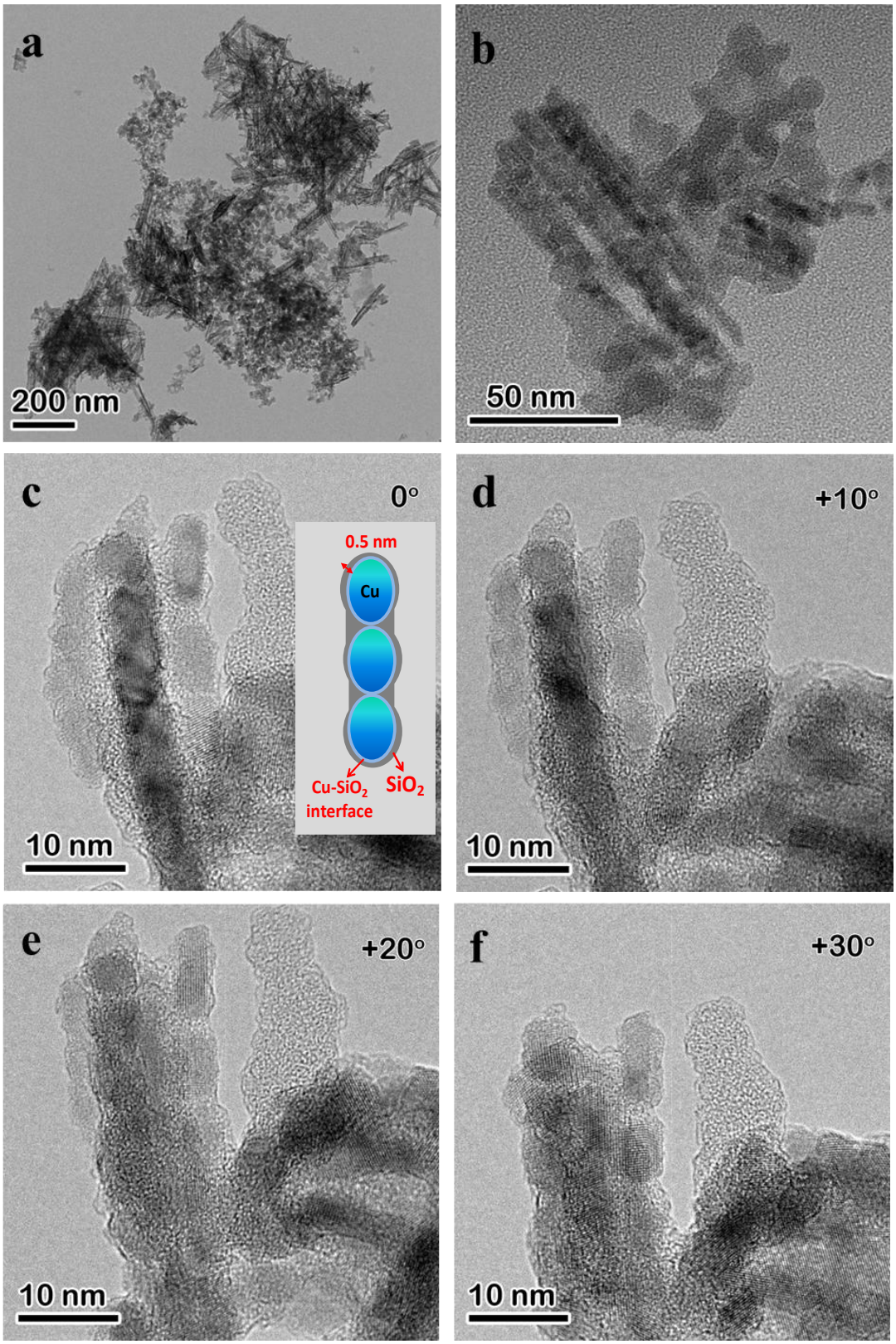

Figure 3. TEM images of the as-calcined CuO/SiO_2 sample and the schematic illustration of the core-shell structure of the rod-like section.

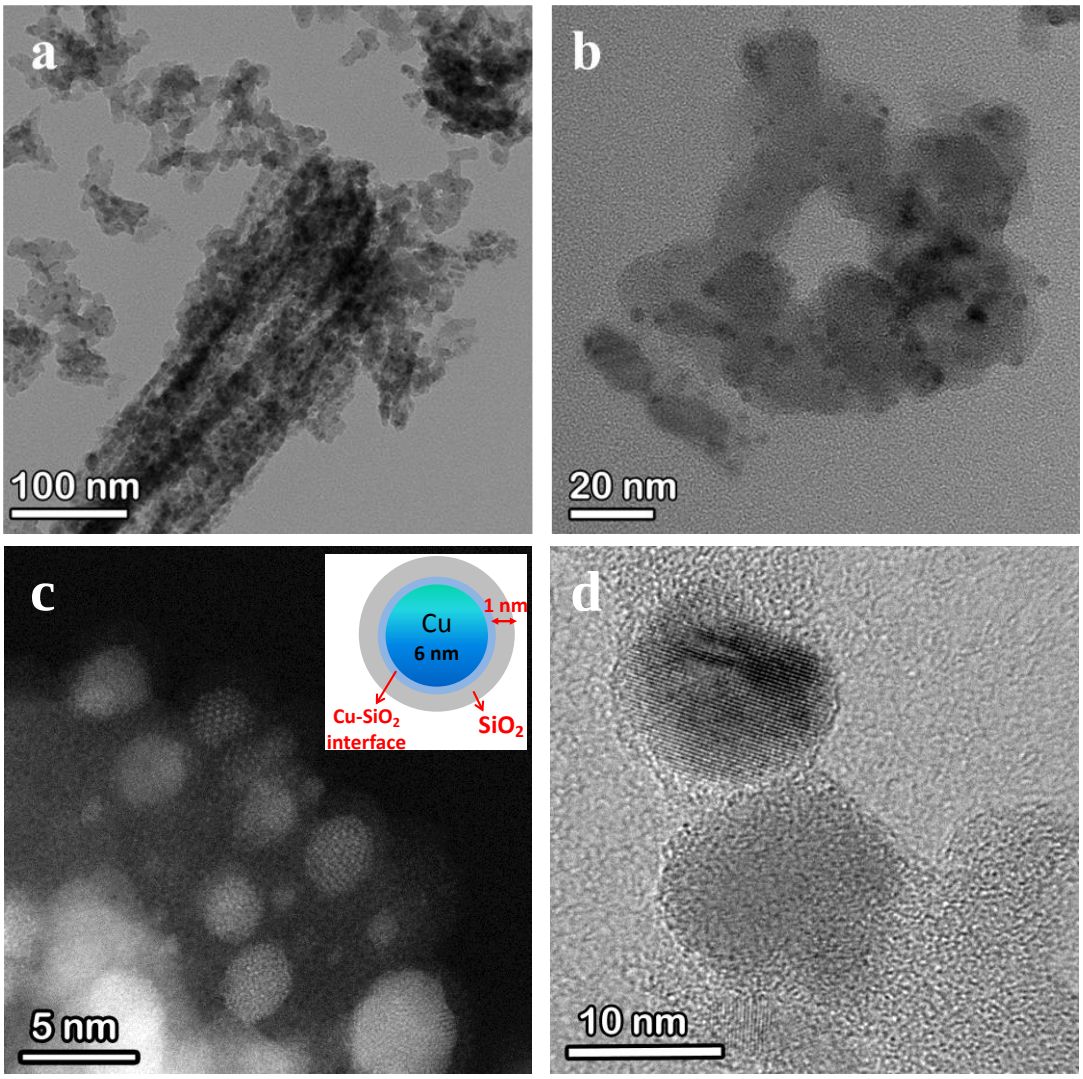

Figure 4. TEM/STEM images of the hydrogen-reduced Cu/SiO_2 catalyst and the schematic illustration of the core-shell structure of the highly dispersed copper particles.

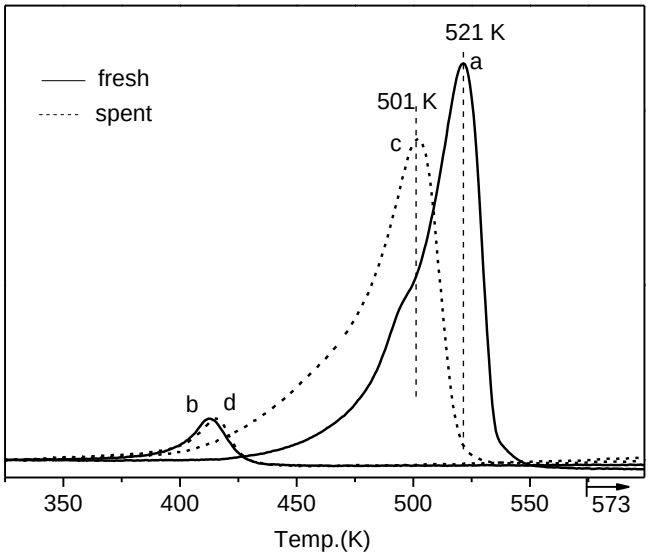

Figure 5. H_2-TPR profiles of the as-calcined CuO/SiO_2 sample and the spent Cu/SiO_2 catalyst. (a) the first reduction profile of the as-calcined fresh CuO/SiO_2 sample, (b) the second reduction profile of the as-calcined fresh Cu/SiO_2 sample after N_2O surface oxidation, (c) the first reduction profile of spent sample, (d) the second reduction profile of the spent sample after N_2O surface oxidation.

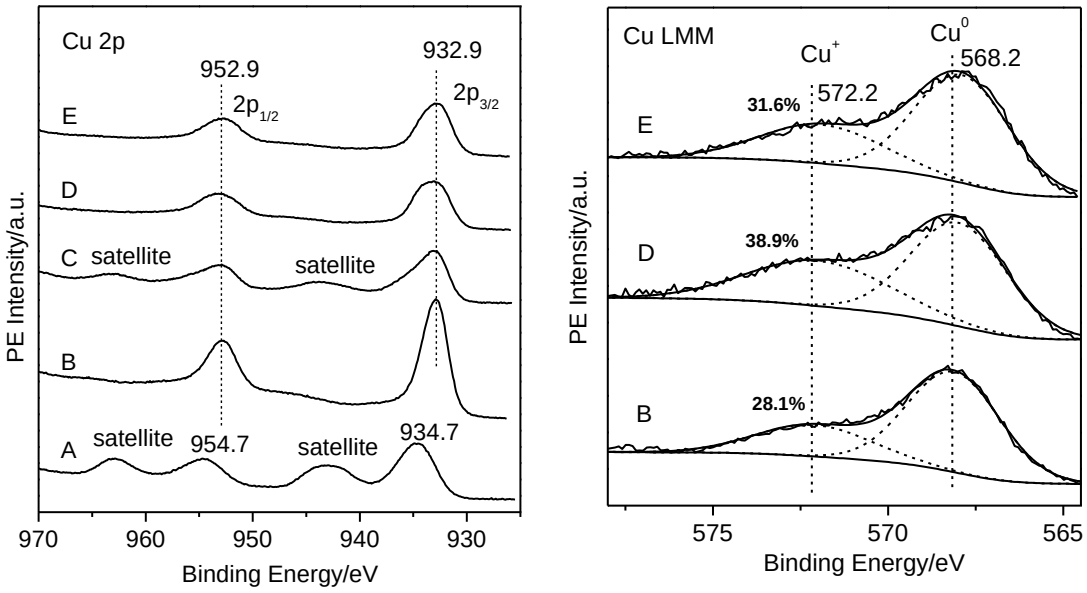

Figure 6. Cu 2p XPS and Cu LMM XAES spectra of (A) the as-calcined CuO/SiO_2 sample, (B) the hydrogen-reduced Cu/SiO_2 catalyst, and (C) the spent Cu/SiO_2 catalyst after passivation and its derived samples after hydrogen-reduction at 483 K (D) and 573 K (E).

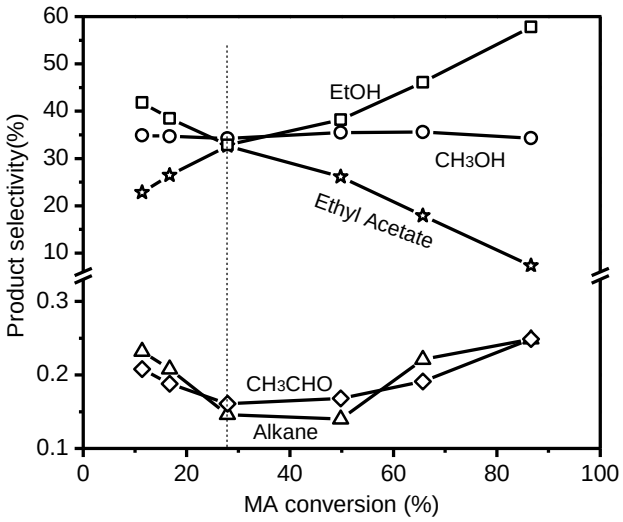

Figure 7. Effect of MA conversion on the product selectivity during MA hydrogenation over the Cu/SiO_2 catalyst. Reaction conditions: 498 K, 1.0 MPa, MA/H_2=2.5/97.5 vol%.

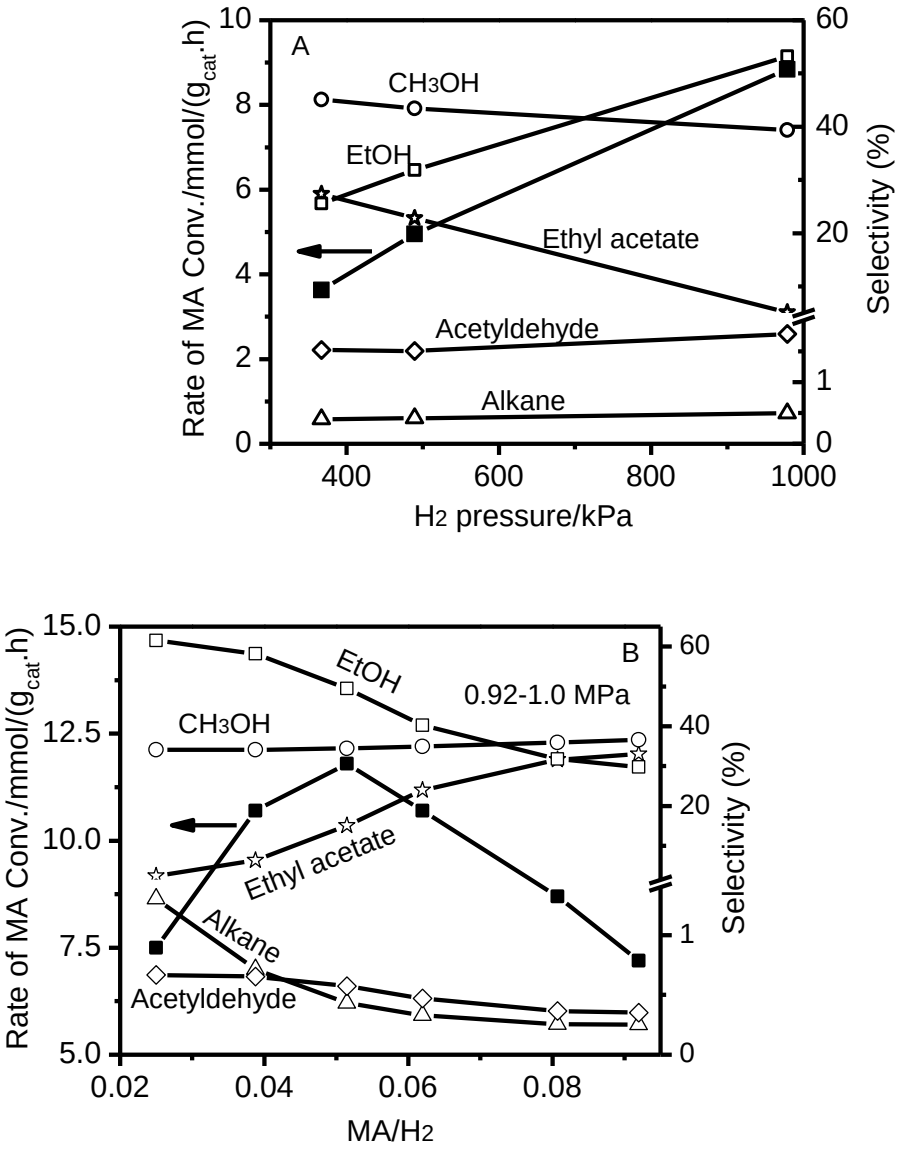

Figure 8. Effects of H_2 (A) and MA (B) partial pressures on the reaction rate and the product selectivity during MA hydrogenation on the Cu/SiO_2 catalyst. Reaction conditions：A: 513 K，P_{MA} = 35 kPa, GHSV = 6000 mL/(g_{cat}·h); B: 523 K, P_{H2} = 920-1000 kPa, GHSV = 6000 mL/(g_{cat}·h).

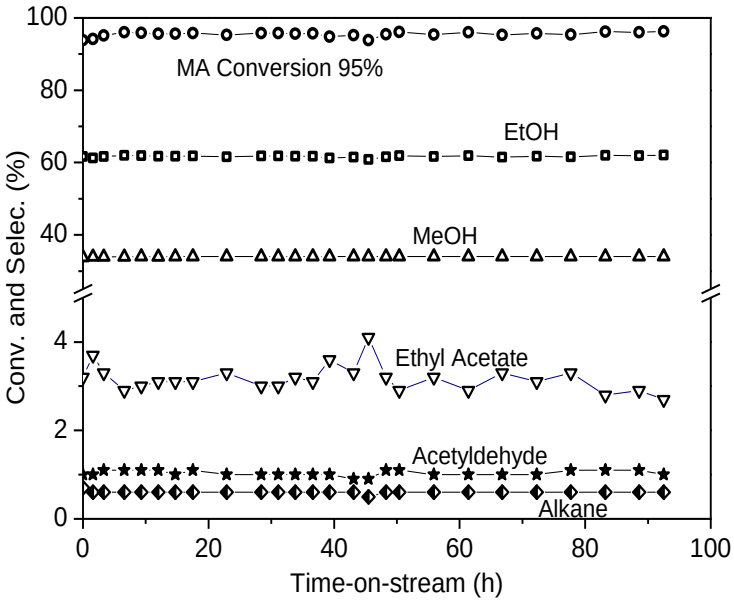

Figure 9. Stability test of the Cu/SiO_2 catalyst for MA hydrogenation. Reaction conditions: 523 K, 1.0 MPa, MA/H_2 = 3/97 vol%, GHSV = 6000 mL/(g_{cat}·h).

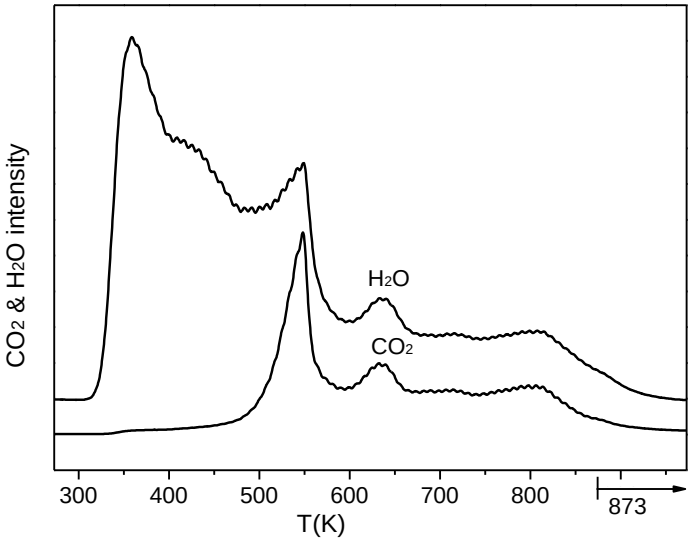

Figure 10. Temperature-programmed desorption profile of the spent Cu/SiO_2 catalyst under He flow.

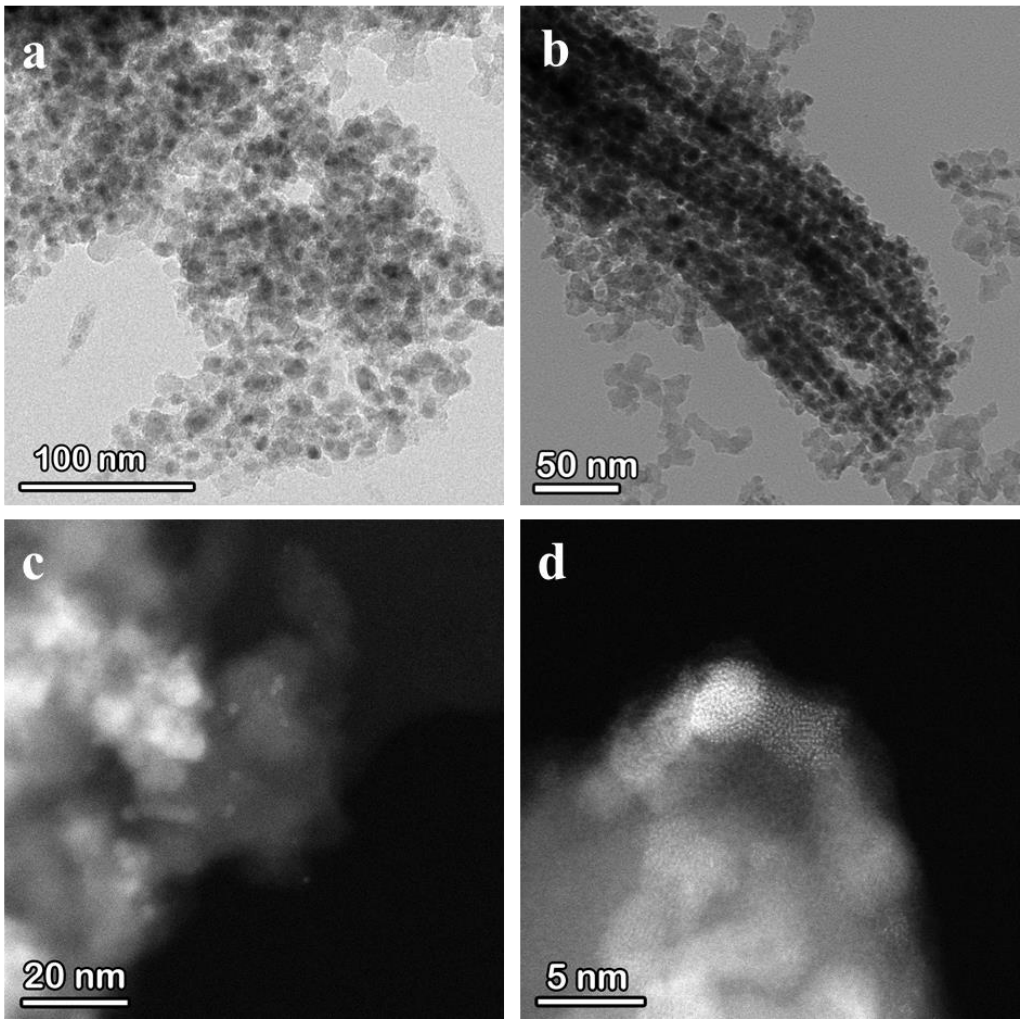

Figure 11. TEM/STEM images of the spent Cu/SiO_2 catalyst.

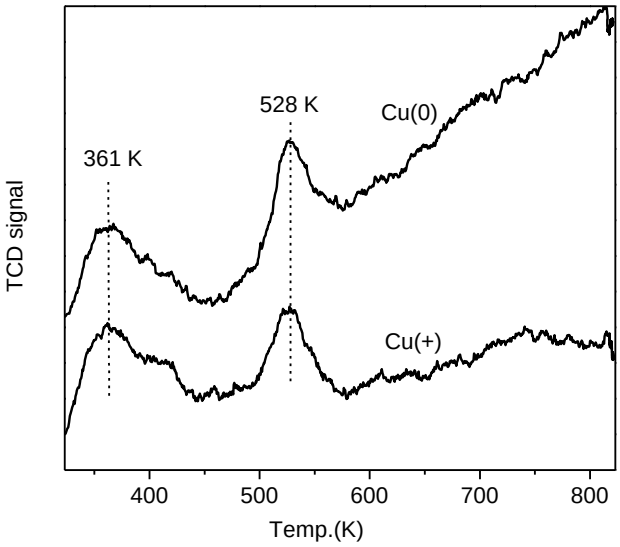

Figure 12. MA-TPD profiles over the referencing Cu/SiO_2 catalysts containing different Cu species. The desorption at 361 K was originated from traces of water in the dosing gas.

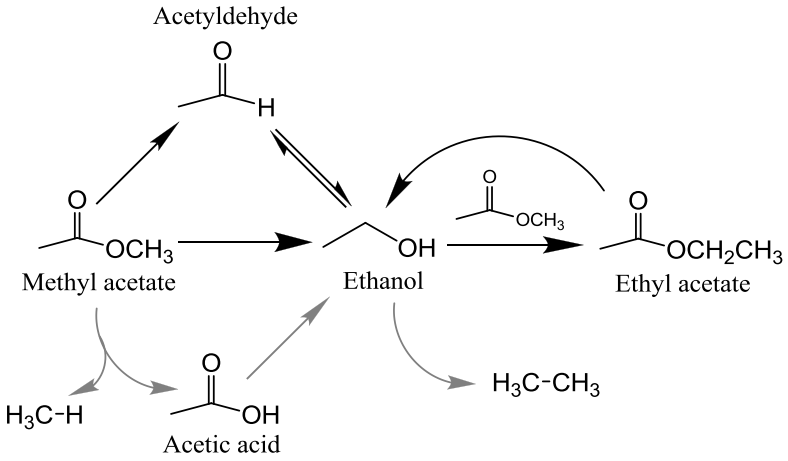

Scheme 1. Possible surface reaction routes for methyl acetate hydrogenation on the Cu/SiO_2 catalyst.

Table 1. Effect of reaction temperature on the catalytic performance of the Cu/SiO_2 catalyst

Temp. (K)	MA Conv.%	Product Selectivity (%)				
		Alkanes*	Acetaldehyde	EtOAc	MeOH	EtOH
493	26.5	0.2 (CH_4)	---	32.7	36.4	30.8
518	81.1	0.4 (50% C_2H_6)	0.2	12.2	34.2	52.9
528	96.2	1.7 (75% C_2H_6)	0.5	2.5	33.6	61.7

Reaction conditions: MA/H_2= 3.5/96.5 vol%, 6000 mL/(g_{cat}·h), 1.0 MPa.

*Data in the brackets indicate the selectivity of C_2H_6 in total alkanes (CH_4+C_2H_6).

Table 2. MA conversion over the Cu/SiO_2 catalyst

Catalyst Loading (g)	MA(l) (μl/min)	H_2 (mL/min)	W/F (g.s/mL)	Contact time (g.h/molMA)	MA Conv.%
0.3	2	17	1.06	274.6	86.6
0.3	4	34	0.53	127.1	49.8
0.3	6	51	0.35	81.9	27.8
0.15	4	34	0.26	68.3	16.7
0.15	6	51	0.18	43.2	11.4

Reaction conditions: 498 K, 1.0 MPa, MA concentration: 2.5% (by GC analysis using a 2% MA/He calibration gas). For a specified loading of catalyst (0.15 or 0.3 g), MA conversion linearly decreased as the feeding rate increased, making the amount of MA converted nearly constant. This suggests that effect of external diffusion is excluded.

Table 3. Results of control experiments on the Cu/SiO_2 catalyst

Reaction	Temp. (K)	Conv. (%)	Sel. (%)				
			Alkane	Acetaldehyde	EtOAc	Methanol	Ethanol
MA+H_2[a]	493	26.5	0.19	0.07	32.6	36.4	30.8
	518	81.1	0.40	0.24	12.2	34.2	52.9
EA+H_2[b]	493	77.3	0.22	0.38	0	0	99.4
	518	91.8	0.93	0.85	0	0	98.2
EtOH+H_2[c]	498	0.6	35(C_2H_6)	65			
EtOH+N_2[d]	498	24	0.5(C_2H_4)	99.5			

[a] MA/H_2 =3.2/96.8 vol%, GHSV = 6000 mL/(g_{cat}·h), 1.0 MPa;

[b] EA/H_2 =3.0/97.0 vol%, GHSV = 6600 mL/(g_{cat}·h), 1.0 MPa;

[c] $EtOH/H_2$ =2.5/97.5 vol%, GHSV = 6600 mL/(g_{cat}·h), 1.0 MPa;

[d] $EtOH/N_2$ =2.5/97.5 vol%, GHSV = 6000 mL/(g_{cat}·h), 0.5 MPa.